






DESIVAST: A Catalog of Low-Redshift Voids using Data from the DESI DR1 Bright Galaxy Survey

HERNAN RINCON ¹ SEGEV BENZVI ¹ KELLY DOUGLASS ¹ DAHLIA VEYRAT ¹ JESSICA NICOLE AGUILAR,²
STEVEN AHLEN ³ DAVIDE BIANCHI ⁴ DAVID BROOKS,⁵ TODD CLAYBAUGH,² SHAUN COLE ⁶
AXEL DE LA MACORRA ⁷ PETER DOEL,⁵ ANDREU FONT-RIBERA ^{5,8} JAIME E. FORERO-ROMERO ^{9,10}
ENRIQUE GAZTAÑAGA,^{11,12,13} SATYA GONTCHO A GONTCHO ² GASTON GUTIERREZ,¹⁴ KLAUS HONSCHEID,^{15,16,17}
CULLAN HOWLETT ¹⁸ STEPHANIE JUNEAU,¹⁹ ROBERT KEHOE,²⁰ SERGEY KOPOSOV ^{21,22} ANDREW LAMBERT,²
MARTIN LANDRIAU ² LAURENT LE GUILLOU ²³ AARON MEISNER ¹⁹ RAMON MIQUEL,^{24,8} JOHN MOUSTAKAS ²⁵
GUSTAVO NIZ ^{26,27} WILL PERCIVAL ^{28,29,30} FRANCISCO PRADA ³¹ IGNASI PÉREZ-RÀFOLS ³² GRAZIANO ROSSI,³³
EUSEBIO SANCHEZ ³⁴ MICHAEL SCHUBNELL,^{35,36} HEE-JONG SEO ³⁷ DAVID SPRAYBERRY,¹⁹ GREGORY TARLÉ ³⁶
BENJAMIN ALAN WEAVER,¹⁹ AND HU ZOU ³⁸

¹Department of Physics & Astronomy, University of Rochester, 206 Bausch and Lomb Hall, P.O. Box 270171, Rochester, NY 14627-0171, USA

²Lawrence Berkeley National Laboratory, 1 Cyclotron Road, Berkeley, CA 94720, USA

³Physics Dept., Boston University, 590 Commonwealth Avenue, Boston, MA 02215, USA

⁴Dipartimento di Fisica “Aldo Pontremoli”, Università degli Studi di Milano, Via Celoria 16, I-20133 Milano, Italy

⁵Department of Physics & Astronomy, University College London, Gower Street, London, WC1E 6BT, UK

⁶Institute for Computational Cosmology, Department of Physics, Durham University, South Road, Durham DH1 3LE, UK

⁷Instituto de Física, Universidad Nacional Autónoma de México, Cd. de México C.P. 04510, México

⁸Institut de Física d’Altes Energies (IFAE), The Barcelona Institute of Science and Technology, Campus UAB, 08193 Bellaterra Barcelona, Spain

⁹Departamento de Física, Universidad de los Andes, Cra. 1 No. 18A-10, Edificio Ip, CP 111711, Bogotá, Colombia

¹⁰Observatorio Astronómico, Universidad de los Andes, Cra. 1 No. 18A-10, Edificio H, CP 111711 Bogotá, Colombia

¹¹Institut d’Estudis Espacials de Catalunya (IEEC), 08034 Barcelona, Spain

¹²Institute of Cosmology and Gravitation, University of Portsmouth, Dennis Sciama Building, Portsmouth, PO1 3FX, UK

¹³Institute of Space Sciences, ICE-CSIC, Campus UAB, Carrer de Can Magrans s/n, 08913 Bellaterra, Barcelona, Spain

¹⁴Fermi National Accelerator Laboratory, PO Box 500, Batavia, IL 60510, USA

¹⁵Center for Cosmology and AstroParticle Physics, The Ohio State University, 191 West Woodruff Avenue, Columbus, OH 43210, USA

¹⁶Department of Physics, The Ohio State University, 191 West Woodruff Avenue, Columbus, OH 43210, USA

¹⁷The Ohio State University, Columbus, 43210 OH, USA

¹⁸School of Mathematics and Physics, University of Queensland, 4072, Australia

¹⁹NSF NOIRLab, 950 N. Cherry Ave., Tucson, AZ 85719, USA

²⁰Department of Physics, Southern Methodist University, 3215 Daniel Avenue, Dallas, TX 75275, USA

²¹Institute for Astronomy, University of Edinburgh, Royal Observatory, Blackford Hill, Edinburgh EH9 3HJ, UK

²²Institute of Astronomy, University of Cambridge, Madingley Road, Cambridge CB3 0HA, UK

²³Sorbonne Université, CNRS/IN2P3, Laboratoire de Physique Nucléaire et de Hautes Energies (LPNHE), FR-75005 Paris, France

²⁴Institució Catalana de Recerca i Estudis Avançats, Passeig de Lluís Companys, 23, 08010 Barcelona, Spain

²⁵Department of Physics and Astronomy, Siena College, 515 Loudon Road, Loudonville, NY 12211, USA

²⁶Departamento de Física, Universidad de Guanajuato - DCI, C.P. 37150, Leon, Guanajuato, México

²⁷Instituto Avanzado de Cosmología A. C., San Marcos 11 - Atenas 202. Magdalena Contreras, 10720. Ciudad de México, México

²⁸Department of Physics and Astronomy, University of Waterloo, 200 University Ave W, Waterloo, ON N2L 3G1, Canada

²⁹Perimeter Institute for Theoretical Physics, 31 Caroline St. North, Waterloo, ON N2L 2Y5, Canada

³⁰Waterloo Centre for Astrophysics, University of Waterloo, 200 University Ave W, Waterloo, ON N2L 3G1, Canada

³¹Instituto de Astrofísica de Andalucía (CSIC), Glorieta de la Astronomía, s/n, E-18008 Granada, Spain

³²Departament de Física, EEBE, Universitat Politècnica de Catalunya, c/Eduard Maristany 10, 08930 Barcelona, Spain

³³Department of Physics and Astronomy, Sejong University, Seoul, 143-747, Korea

³⁴CIEMAT, Avenida Complutense 40, E-28040 Madrid, Spain

hrincon@ur.rochester.edu

segev.benzvi@rochester.edu

kellyadouglass@rochester.edu

dveyrat@ur.rochester.edu

³⁵*Department of Physics, University of Michigan, Ann Arbor, MI 48109, USA*

³⁶*University of Michigan, Ann Arbor, MI 48109, USA*

³⁷*Department of Physics & Astronomy, Ohio University, Athens, OH 45701, USA*

³⁸*National Astronomical Observatories, Chinese Academy of Sciences, A20 Datun Rd., Chaoyang District, Beijing, 100012, P.R. China*

ABSTRACT

We present three separate void catalogs created using a volume-limited sample of the DESI DR1 Bright Galaxy Survey. We use the algorithms VoidFinder and V^2 to construct void catalogs out to a redshift of $z = 0.24$. We obtain 1,484 interior voids with VoidFinder, 386 with V^2 using REVOLVER pruning, and 295 with V^2 using VIDE pruning. Comparing our catalog with an overlapping SDSS void catalog, we find generally consistent void properties but significant differences in the void volume overlap, which we attribute to differences in the galaxy selection and survey masks. These catalogs are suitable for studying the variation in galaxy properties with cosmic environment and for cosmological studies.

1. INTRODUCTION

On large scales, the structure of the universe is organized into a complex cosmic web consisting of dense clusters and filaments and underdense voids (Gregory & Thompson 1978; Jöeveer et al. 1978; Springel et al. 2006; van de Weygaert 2014; Libeskind et al. 2018). This large-scale structure is the result of the gravitational collapse of matter following initial inhomogeneities in the primordial universe (Bernardeau et al. 2002; Cautun et al. 2014). In the present era, cosmic voids occupy a majority of the universe’s volume, with sizes on the order of tens of Mpc (van de Weygaert & Platen 2011; Jennings et al. 2013; Douglass et al. 2023). Voids evolve under the combined effects of gravity, which expels their matter content, and dark energy, which dominates their expansion at an earlier time compared to surrounding dense regions (Sheth & van de Weygaert 2004; Demchenko et al. 2016). In this way, voids are dynamically unique objects.

Voids provide a cosmological probe for models of dark energy and modified gravity (van de Weygaert 2014; Pisani et al. 2019). The on-average spherical shape of voids makes them well-suited for Alcock-Paczynski tests of cosmology (Alcock & Paczynski 1979; Sutter et al. 2012a, 2014b; Nadathur et al. 2019). The theoretical distribution of void sizes, known as the void size function, is a probe of dark energy (Sheth & van de Weygaert 2004; Jennings et al. 2013; Pisani et al. 2015; Contarini et al. 2022, 2023; Song et al. 2024). The void size function and void density profiles also serve as tests of modified gravity (Voivodic et al. 2017; Perico et al. 2019).

The constraining power of void-based cosmological tests benefits from large void catalogs. Recent years have seen void catalogs built using galaxies from the Sloan Digital Sky Survey (SDSS) (Pan et al. 2012; Sutter et al. 2012b; Nadathur 2016; Mao et al. 2017; Achitouv 2019; Hamaus et al. 2020; Douglass et al. 2023),

with SDSS providing spectroscopy for millions of galaxies and quasars out to redshifts past $z > 2$ (Abazajian et al. 2009; Abdurro’uf et al. 2022). Compared to SDSS, the Dark Energy Spectroscopic Instrument (DESI) Survey will provide a new benchmark for galaxy-redshift surveys, with measured redshifts for over 40 million targets out to redshifts past $z > 3$ (DESI Collaboration et al. 2016a,b). DESI uses four distinct spatially overlapping classes of galaxies to probe a large range of cosmic history. Compared to SDSS, void catalogs built with DESI will contain significantly higher void counts and will trace the evolution of voids over a larger interval of cosmic time.

Making full use of DESI galaxies in the construction of void catalogs requires consideration of the survey target selection. DESI tracers are selected using magnitude and color (Hahn et al. 2023; Zhou et al. 2023; Raichoor et al. 2023; Chaussidon et al. 2023), and the resulting change in tracer density with redshift and tracer type must be accounted for by void-finding algorithms.

Previous void catalogs have accounted for the variation in tracer density with redshift by restricting their void-finding to low-redshift, volume-limited galaxy samples (Pan et al. 2012; Douglass et al. 2023), or by weighting the performance of the void-finding algorithms with respect to the tracer density as a function of redshift (Nadathur 2016; Mao et al. 2017; Hamaus et al. 2020). While galaxy-weighting has the advantages of obtaining a larger void sample and probing a greater range of cosmic history, it comes with the limitation of detecting artificially large voids due to the mean galaxy separation exceeding the expected void sizes (Mao et al. 2017). Void catalogs built with SDSS at high redshift tend to find an abundance of voids with radii greater than 30 Mpc h^{-1} (Sutter et al. 2012b; Nadathur 2016), whereas low-redshift, volume-limited catalogs tend to find an abundance of voids around the range of 15-20

Mpc h⁻¹ (Pan et al. 2012; Douglass et al. 2023), contrary to theoretical expectations. We expect void sizes to increase with decreasing redshift as we trace the evolution of expanding underdensities¹ (Sheth & van de Weygaert 2004). That we instead see larger voids at higher redshifts may be indicative of the challenge of overcoming Malmquist bias when using galaxies to identify low-density regions in the cosmic web (Sutter et al. 2014a).

An accurate description of void sizes is important to astrophysical studies that observe the variation of galaxy properties with cosmic environment (Patiri et al. 2006; Zaidouni et al. 2024). In addition to high redshift void catalogs, there is good reason for creating low-redshift, volume-limited catalogs, where we have the highest confidence in our ability to identify low-density voids.

In this paper, we present a low-redshift void catalog built on the DESI Bright Galaxy Survey (BGS). We use BGS Bright galaxies within $z \leq 0.24$ to construct void catalogs with two void-finding algorithms: the sphere-growing algorithm VoidFinder (El-Ad & Piran 1997; Hoyle & Vogeley 2002) and the watershed algorithm ZOBOV (Neyrinck 2008), titled V² in our implementation.

Our void catalogs are collected in the DESIVAST value added catalog. DESIVAST DR1 will be publicly released with DESI DR1. Our void catalogs will be updated with each data release; we here present results for DESI DR1.

This paper is structured as follows. Section 2 discusses the void-finding algorithms used for the void catalog construction. Section 3 discusses the creation of a volume-limited galaxy catalog from DESI BGS galaxies. Section 4 presents the void catalogs and compares the catalogs across different void-finding algorithms and to voids found in the common volume observed with SDSS. Section 5 concludes and sets the scope for future iterations of DESIVAST.

2. VOID-FINDING ALGORITHMS

We perform void-finding with the sphere-growing algorithm VoidFinder (El-Ad & Piran 1997; Hoyle & Vogeley 2002) and the watershed ZOBOV algorithm (Neyrinck 2008), here titled V². We use implementations of these two algorithms in the Void Analysis Software Toolkit (VAST; Douglass et al. 2023).

¹ Voids may contract over time when embedded within a larger, overdense region. This so-called “void-in-cloud” process affects the shape of the void size distribution, while the average void size increases with time (van de Weygaert 2014).

VoidFinder uses a volume-limited galaxy sample for void construction. The algorithm partitions the input galaxy sample into highly clustered “wall” regions and isolated “field” regions. Voids are defined to contain field galaxies and to be bordered by wall galaxies. The wall-field classification of galaxies is made based on the third-nearest neighbor of each galaxy, where galaxies that have a third-nearest neighbor above a threshold distance are identified as field galaxies. The threshold distance is taken to be $d = \bar{d} + 1.5\sigma$, where \bar{d} is the average third-nearest neighbor separation, and σ is its standard deviation. The algorithm removes all field galaxies so that voids may be identified in the “hole” regions left behind. The algorithm then defines a fine grid over the volume, typically with a resolution of around 1 Mpc h⁻¹, and seeds spheres in all empty grid cells. The spheres are grown until they are bordered by four wall galaxies. The largest resulting spheres that do not overlap with any larger sphere are labeled as “maximal spheres” and are identified with individual voids. All remaining spheres that overlap 50% of their volume with a maximal sphere are then merged with the maximal sphere, allowing for VoidFinder voids to describe the complex shapes expected from real voids, rather than modeling each void as a simple sphere (El-Ad & Piran 1997; Hoyle & Vogeley 2002; Douglass et al. 2023).

In contrast to VoidFinder, V² may use a magnitude-limited galaxy sample. The algorithm uses the galaxy density field to define voids, which is calculated by applying a Voronoi tessellation to the galaxy catalog. The volume of a galaxy’s Voronoi cell is used to estimate the local density. In the case of a magnitude-limited survey, the density for each cell can be weighted by the survey selection function. We have not applied such weights and therefore restrict ourselves to a volume-limited sample. The algorithm then identifies low density basins of adjacent cells, termed “zones”, each of which are separated by high density ridges. Various combinations of zones may be defined as voids, and there exist differing treatments for combing zones, referred to as pruning methods. The VIDE pruning method (Sutter et al. 2015) uses a minimum linking density threshold between adjacent zones to determine which zones should be combined into voids and applies an optional central-density cut to the final catalog. The REVOLVER pruning method doesn’t combine any zones and instead treats all individual zones as voids (Nadathur et al. 2019). The VAST software suite includes both pruning methods, referred to as V_{VIDE}² and V_{REVOLVER}². Any Voronoi cell extending outside of the survey mask is given an infinite density so as to prevent voids from exceeding the survey boundaries.

VoidFinder voids have been shown to correspond to dynamically distinct regions with low shell-crossing numbers (Veyrat et al. 2023). In comparison, V^2 voids are known to include wall features within the void volumes and combine adjacent dynamically distinct void regions into single voids. As result of these differences, VoidFinder voids tend to be smaller and more numerous than V^2 voids. VoidFinder voids have also been shown to contain galaxies that are bluer, fainter, and have higher specific star formation rates than the surrounding wall galaxies (Zaidouni et al. 2024). V^2 voids in contrast contain galaxies with no notable differences from those in wall regions.

The ability of VoidFinder to identify dynamically distinct regions with unique galaxy properties and the ability of V^2 to identify a hierarchy of voids through different pruning methods gives each algorithm advantages for creating a low-redshift void catalog. We thus use both. Here, we focus on a comparison of the two void-finding algorithms on the same volume-limited catalog of DESI DR1 data.

3. DATA AND SELECTION

The Dark Energy Spectroscopic Instrument (DESI) is an ongoing, state-of-the-art galaxy-redshift survey that will cover 14,000 deg² of the sky and measure the redshifts of over 40 million galaxies and quasars out to $z > 3$ (Levi et al. 2013; DESI Collaboration et al. 2016a). DESI has carried out the 3-band Legacy Imaging Survey (Dey et al. 2019), from which targets have been selected for an ongoing 360–980 nm spectroscopic survey, conducted with the DESI instrument on the Mayall Telescope at Kitt Peak National Observatory (DESI Collaboration et al. 2016b, 2022; Silber et al. 2023; Miller et al. 2023). DESI targets include overlapping populations of nearby bright galaxies, (Hahn et al. 2023), luminous red galaxies (Zhou et al. 2023), emission line galaxies (Raichoor et al. 2023), and quasars (Chaussidon et al. 2023). To facilitate a complex survey with multiple target classes, DESI has extensive data collection and processing pipelines, including procedures for survey-tiling (Schlafly et al. 2023), spectroscopic reduction (Guy et al. 2023a), and redshift-fitting (Bailey et al. 2024).

DESI has completed survey validation (DESI Collaboration et al. 2024a), an early data release (Collaboration et al. 2024), and DR1 data collection (DESI Collaboration et al. 2024b). DR1 science results include two point clustering measurements (DESI Collaboration et al. 2024c), Baryon Acoustic Oscillations (BAO) from galaxies and quasars (DESI Collaboration et al. 2024d) and from the Lyman-alpha forest (DESI Collab-

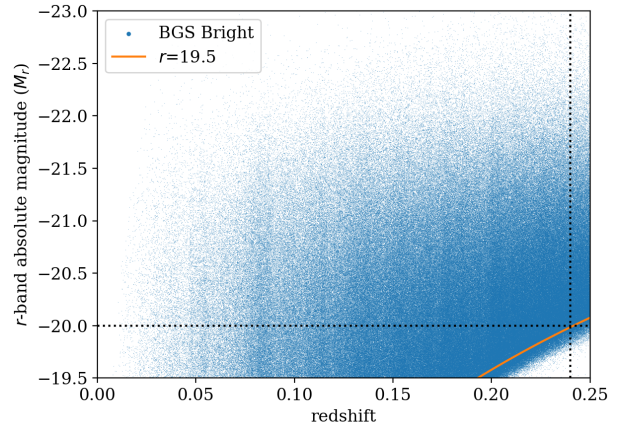


Figure 1. A magnitude-redshift diagram for BGS Bright galaxies, with K-corrections and E-corrections applied. The magnitude and redshift boundaries for the volume-limited sample are shown as dashed lines. The survey apparent magnitude limit is shown as an orange line.

oration et al. 2024e), full-shape analysis from galaxies and quasars (DESI Collaboration et al. 2024f), and cosmological constraints from both BAO (DESI Collaboration et al. 2024e) and full-shape measurements (DESI Collaboration et al. 2024g).

We construct a volume-limited catalog from the DESI DR1 BGS Bright survey (Hahn et al. 2023) as the galaxy input for our void-finding. We select galaxies brighter than $M_r \leq -20$, a population that is known to trace large-scale structure (Pan et al. 2012).

We obtain K-corrections for the galaxies from the FastSpecFit Value Added Catalogs (Moustakas et al. 2023; Moustakas 2024, in preparation). We select synthesized SDSS r -band absolute magnitudes (M_r) that are K-corrected to $z = 0.1$. We add an evolutionary (E) correction centered at the same redshift, $E(z) = -Q_0(z - 0.1)$, with the intention of selecting galaxies at different redshifts that trace the same large-scale structure. The scale factor Q_0 is chosen as $Q_0 = 0.97$, following the calibration from McNaught-Roberts et al. (2014).

With K-corrections and E-corrections applied, our $M_r \leq -20$ magnitude cut corresponds to a redshift limit of $z \leq 0.24$, the maximum distance at which $M_r = -20$ galaxies can be observed by the BGS Bright survey. This distance limit is a consequence of the $r \leq 19.5$ apparent magnitude limit for BGS Bright. A magnitude-redshift plot of the galaxies and the selections for the volume-limited catalog are shown in Figure 1.

The DR1 catalog has uneven angular coverage on the sky, with coverage consisting of one to four overlapping survey tiles. To minimize the effect of this variation, we impose an angular mask selecting only regions where all

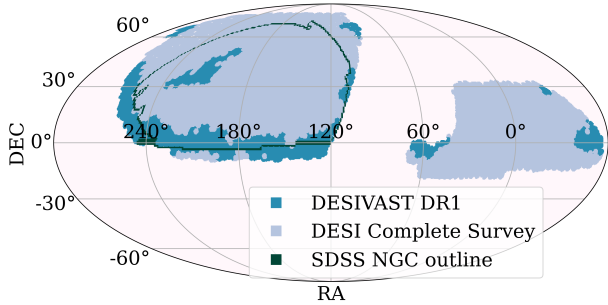


Figure 2. The angular mask used for the DESIVAST DR1 void catalogs, shown in teal. The complete DESI survey mask is shown in gray. For comparison, an outline of the SDSS NGC, which overlaps with the DESI NGC, is shown in dark green.

planned survey tiles for up to four passes have been observed. As DESI is an ongoing survey, this mask has many small, non-contiguous regions. We then use a smoothed version of the mask to select voids for our final catalogs. To smooth our mask, we convolve it with a Gaussian filter with $\sigma = 2.8^\circ$. This convolution assigns each pixel a weight between 0 and 1. We keep mask pixels whose weights are greater than 0.34, finding that the resulting mask removes small, non-contiguous regions while preserving the survey edges. This final angular mask is shown in Figure 2 (labeled DESIVAST DR1) and covers a region of 2320 (386) deg^2 in the North (South) Galactic Cap.

DESI redshifts are fitted using the Redrock software package (Guy et al. 2023b). Redrock includes several fit quality indicators, notably a ZWARN flag that indicates a lack of confidence in the fit or errors in the fitting procedure, and a $\Delta\chi^2$ (DELTA CHI2) indicator of how confidently the software has chosen the correct spectral classification for each spectral fit. To ensure accurate redshifts, we select only galaxies with no raised ZWARN flags and require $\Delta\chi^2 > 45$ for confident spectral classification.

The angular mask and redshift cuts reduce the BGS DR1 sample from an initial count of 4,741,408 galaxies to a subsequent count of 1,217,372 galaxies. The $M_r \leq -20$ magnitude cut further reduces the sample to 488,334 galaxies. The spectroscopic quality cuts impose a minimal reduction in the galaxy sample size of 0.01%. Our final volume-limited catalog contains 483,293 galaxies, with 402,642 in the North Galactic Cap (NGC), and 80,651 in the South Galactic Cap (SGC). The resulting survey volume is 0.085 Gpc^3 .

3.1. SDSS DR7 Galaxies

The Sloan Digital Sky Survey (SDSS; York et al. 2000) was the most ambitious galaxy-redshift survey prior to

DESI, conducted with the 2.5 m Sloan Foundation Telescope at the Apache Point Observatory (Gunn et al. 2006). SDSS included a 5-band photometric imaging survey (Fukugita et al. 1996) and a 380–920 nm spectroscopic survey (Strauss et al. 2002), for overlapping populations of bright galaxies (Strauss et al. 2002), luminous red galaxies (LRGs) (Eisenstein et al. 2001), and quasars (Richards et al. 2002). The seventh data release (SDSS DR7; Abazajian et al. 2009) of SDSS presents the complete bright galaxy and LRG samples of the survey’s first two stages, SDSS-I/II. These catalogs provide photometry for 357 million objects and 1.6 million spectra. Further data releases past SDSS DR7 do not provide additional high-tracer density, magnitude-complete samples, making SDSS DR7 the most recent galaxy-redshift survey suitable for a comparison with the DESIVAST sample.

SDSS DR7 covers a contiguous 7,500 deg^2 region in the NGC (Abazajian et al. 2009), providing significant overlap with the complete DESI survey. We are interested in the consistency of voids found between the two surveys in their common region. Given 1,860 deg^2 overlap between the DESIVAST DR1 and SDSS NGC footprints, we are limited in DESIVAST DR1 by the number of SDSS voids that can be compared against DESI voids. However, it is still instructive to compare the two catalogs.

To enable comparisons between DESI and SDSS, we construct a volume-limited catalog of SDSS galaxies from the NASA-Sloan Atlas (NSA; Blanton et al. 2011). Version 1.0.1 of the NSA catalog provides spectroscopy for 641,409 galaxies in SDSS DR7. The SDSS DR7 void catalog of Douglass et al. (2023) is built from the NSA galaxy catalog, K-corrected to $z = 0.0$ and with no applied evolutionary correction. For our own SDSS void catalogs, we chose to K-correct the NSA catalog to $z = 0.1$ and to apply an evolutionary correction $E(z) = -0.97(z - 0.1)$, consistent with that used in DESIVAST.

An absolute magnitude cut of $M_r \leq -20$ imposes a $z \leq 0.114$ redshift limit, the maximum distance at which $M_r = -20$ galaxies can be observed by the SDSS Main Galaxy Survey. We additionally impose an angular mask on the NSA catalog. The mask, shown in Figure 2, selects galaxies within the SDSS NGC.

Our angular mask and redshift cut select 379,405 galaxies from the NSA catalog. Our $M_r \leq -20$ magnitude cut selects a final population of 177,407 galaxies.

3.2. The Impact of DESI and SDSS Galaxies on Voids

The completeness of SDSS and DESI affect their resulting void catalogs. The SDSS Main Galaxy Sample

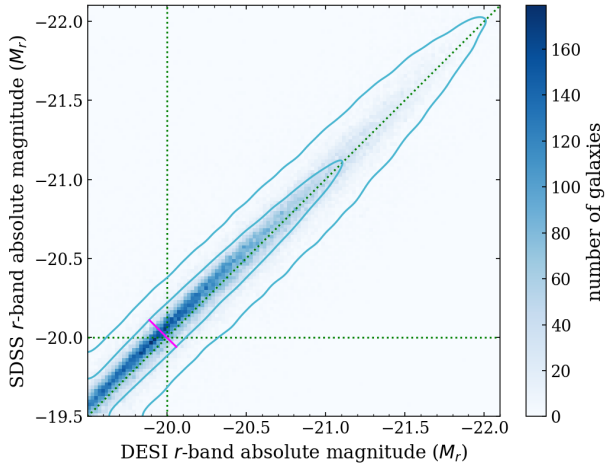


Figure 3. A two-dimensional histogram comparing the r -band magnitudes of galaxies reported by DESI and SDSS. The ideal of a one-to-one relation and the $M_r = -20$ magnitude thresholds are shown as dashed lines. The 68% confidence interval at $M_r = -20$ is shown in magenta.

(MGS) is $>99\%$ complete down to an r -band apparent magnitude of $r \leq 17.77$, though 6% of the sample lacks spectroscopy due to fiber collisions (Strauss et al. 2002). DESI BGS has $>80\%$ fiber assignment completeness down to an r -band apparent magnitude of $r \leq 19.5$ in its original four-pass program (Hahn et al. 2023). Both DESI BGS and SDSS MGS have high redshift success rates such that almost all observed targets have successful redshifts.

When considering a volume-limited galaxy sample, we obtain fewer DESI galaxies than SDSS galaxies. This has the expected effect of producing larger voids in DESI than SDSS, as the wall regions bordering VoidFinder voids will lose galaxies and the watershed ridges bordering V^2 voids will lose resolution.

To directly compare the volume-limited galaxy populations of the two surveys, we smooth the common DESIVAST-SDSS mask to 345 deg^2 , thereby reducing edge effects. Our smoothing follows the same procedure used in section 3, except we only keep mask pixels with weights greater than 0.99 in order to remove regions near the survey edges. In the resulting fiducial volume extending to $z = 0.114$, we find that BGS galaxies have an average separation of 5.62 Mpc, while NSA galaxies have an average separation of 5.20 Mpc.

The DESI and SDSS galaxy samples used for void-finding are also affected by the galaxy magnitudes reported in each survey. In Figure 3, we compare the magnitudes reported by the FastSpecFit VAC and the NSA catalog for matched galaxies. There is scatter in the agreement of the magnitudes, as well as a systematic offset, which affects which galaxies make the $M_r \leq -20$

cut for each survey and ultimately impacts the resulting void catalogs. The upper-left region of the plot, bounded by dashed green lines, shows galaxies included in SDSS but not DESI, and the lower-right region of the plot shows galaxies included in DESI but not SDSS. We see that at $M_r = -20$, galaxies tend to be reported as brighter in SDSS than in DESI. This has the effect of including more galaxies in the SDSS volume-limited catalog compared to DESI, once again suggesting that SDSS voids will be smaller than DESI voids.

We compare the galaxy membership of SDSS and DESI in our smoothed fiducial volume. We find that 30.80% of SDSS galaxies are not present in DESI. When accounting for galaxies that pass the $M_r \leq -20$ threshold for SDSS but not DESI, we find that 24.69% of SDSS galaxies are not present in DESI. Similarly, we find that 12.58% of DESI galaxies are not present in SDSS. Accounting for galaxies that pass the $M_r \leq -20$ threshold for DESI but not SDSS, we find that 10.82% of DESI galaxies are not present in SDSS.

3.3. Mock Galaxy Catalogs

To estimate the impact of statistical uncertainties and cosmic variance on DESI void catalog properties, we use simulated alternate Merged Target Ledgers (AMTL) BGS galaxy catalogs. These AMTL catalogs simulate DESI fiber assignment (Lasker et al. 2024) on mock catalogs (DESI Collaboration et al. 2024d) derived from the AbacusSummit N-body simulation suite (Maksimova et al. 2021; Garrison et al. 2021; Hadzhiyska et al. 2022). We select 25 AMTL catalogs with a cosmology using $\Omega_m = 0.315$, $\Omega_\Lambda = 0.685$, and $H_0 = 67.32 \text{ km s}^{-1} \text{ Mpc}^{-1}$ (Planck Collaboration et al. 2020). The AMTL galaxies include r -band absolute magnitudes that allow us to apply the DESIVAST volume-limited catalog creation procedure to each mock. We take the spread in void properties across mocks to represent the effect of statistical uncertainties and cosmic variance on our void catalogs.

To provide projections for a complete DESI survey BGS void catalog, we use a mock BGS galaxy catalog (DESI Collaboration et al. 2024d) derived from the AbacusSummit N-body simulation suite. We apply the complete DESI survey mask and the DESIVAST redshift limit to the mock catalog to obtain the desired survey volume.

To estimate the impact of statistical uncertainties and cosmic variance on SDSS voids, we use 25 galaxy mocks (Hong et al. 2016) built from the Horizon Run 4 N-body simulation (Kim et al. 2015). The Horizon Run 4 mocks are built on a cosmology with $\Omega_m = 0.241$, $\Omega_\Lambda = 0.759$, and $H_0 = 71.9 \text{ km s}^{-1} \text{ Mpc}^{-1}$ (Dunkley et al. 2009).

The galaxy mocks include a mass estimate that serves as a proxy for luminosity. We apply the SDSS NGC angular mask, distance limits, and magnitude cut to each mock to create volume-limited catalogs. The spread in the resulting void properties is taken to represent the effect of statistical uncertainties and cosmic variance.

As the Horizon Run 4 and Abacus AMTL galaxy mocks use different cosmologies, we limit their use to comparing the variance, and not the expected value, of void catalog properties.

4. THE DESIVAST DR1 VOID CATALOG

We construct three DESI void catalogs, one each for VoidFinder, V^2_{VIDE} , and V^2_{REVOLVER} voids. We assume a cosmology with $\Omega_m = 0.315$, $\Omega_\Lambda = 0.685$, and $H_0 = 67.32 \text{ km s}^{-1} \text{ Mpc}^{-1}$ (Planck Collaboration et al. 2020) to convert galaxy redshifts to comoving distances. For all catalogs, we impose a minimum radius cut to remove voids that are more likely to be Poisson-fluctuated underdensities in the galaxy distribution (see Hoyle & Vogeley (2002) for details). In practice, we require VoidFinder maximal spheres to have a radius larger than 10 Mpc h^{-1} , following a cut optimized for SDSS by Pan et al. (2012). Given our similar target density in BGS at the redshifts being investigated, we apply the same cut to the DESIVAST DR1 sample. Similarly, we cut V^2 voids whose effective spherical radii are smaller than 10 Mpc h^{-1} .

The physical distribution of voids resulting from each algorithm is shown in Figure 4, displayed in a cross-section of the catalogs at a declination of 3° . Voids that fall near the survey boundaries, termed “edge voids”, are drawn in yellow. The remaining interior voids are drawn in blue. We also show galaxies that fall within 5 Mpc h^{-1} of the cross sectional plane, rendered in black (red) when they fall exterior (interior) to voids. For comparison, we show the distance limit of the Douglass et al. (2023) SDSS void catalogs, demonstrating the improved depth of redshift coverage with DESI.

Qualitatively, VoidFinder voids appear smaller and more numerous than V^2 voids, and V^2 voids appear more likely to include wall galaxies within voids, particularly for V^2_{REVOLVER} . This behavior is consistent with the known properties of voids for each algorithm; VoidFinder voids enclose dynamically distinct regions, while V^2 voids combine multiple VoidFinder voids into single objects (Douglass et al. 2023; Veyrat et al. 2023).

V^2_{VIDE} voids appear to fill less of the survey volume than V^2_{REVOLVER} voids due to the central density cut that is (optionally) part of V^2_{VIDE} . Following the convention in Sutter et al. (2015), we remove V^2_{VIDE} void candidates with a central density that is higher than the

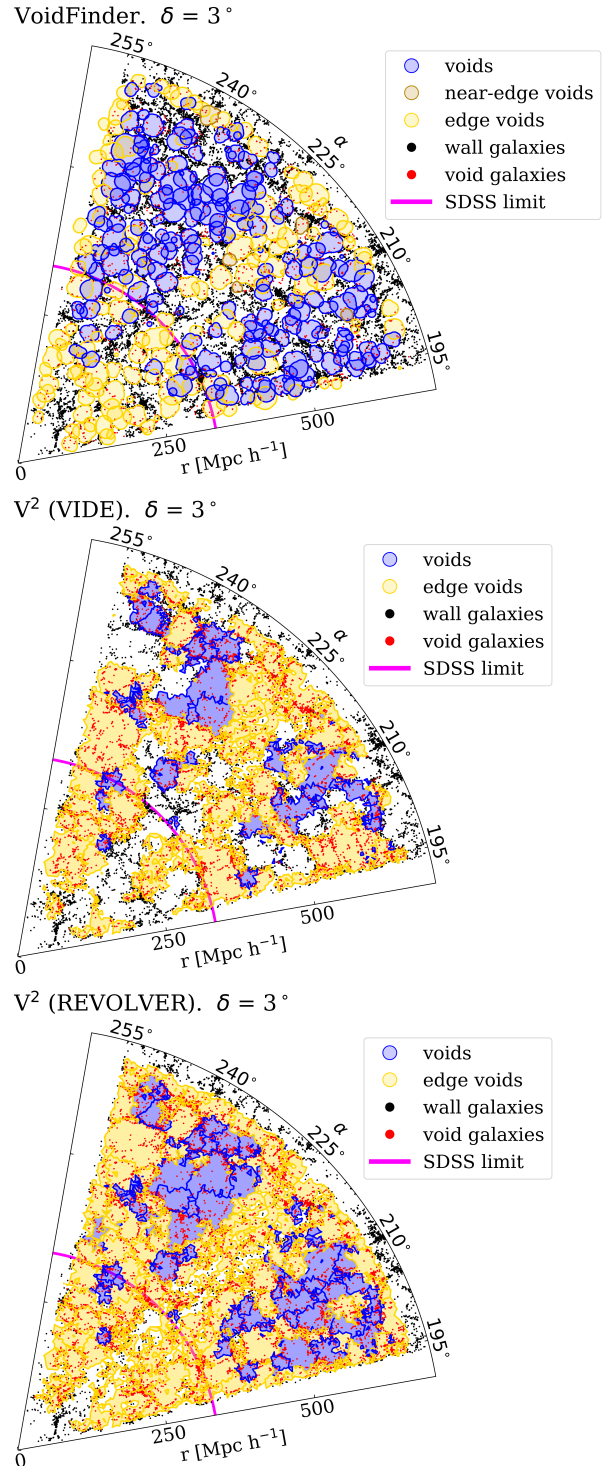


Figure 4. Slice plots of the three void catalogs (from top to bottom: VoidFinder, V^2_{VIDE} , V^2_{REVOLVER}) overlaid on the same survey region. A 10 Mpc h^{-1} thick slice of galaxies is plotted over the void distribution at a declination of $\delta = 3^\circ$. Void (wall) galaxies are shown in red (black). Edge (interior) voids are shown in yellow (blue). We show a comparison with the redshift limit of the Douglass et al. (2023) SDSS void catalogs (solid magenta line).

V_{VIDE}^2 minimum zone-linking density. V^2 , being a watershed algorithm, is designed to fill 100% of the survey volume with voids. The non-void regions seen in both V^2 catalogs are due to our central density and minimum-size cuts.

Edge voids occur because our void-finding algorithms define voids based on the galaxy distribution. The galaxy survey boundaries impact the accurate detection of voids, distorting the shapes of voids in their vicinity, making it useful to identify voids near the survey edge. We define edge voids for VoidFinder as those whose volumes exceed the survey boundaries. For VoidFinder alone, we additionally identify a class of so-called “near-edge voids” that are contained by the survey but have at least one hole falling within 10 Mpc h^{-1} of the survey boundaries. For V^2 , voids do not exceed survey boundaries by construction, and we identify edge voids as those with over 10% of their surface area touching the survey boundary. This definition separates two distinct populations of voids: those with minimal contact with the survey boundaries, and those with significant contact with the survey boundaries. Douglass et al. (2023) showed that this edge void definition accurately identifies V^2 voids whose volumes are impacted by the survey boundaries.

For comparison to DESI voids, we construct three SDSS void catalogs, one each for VoidFinder, V_{VIDE}^2 , and V_{REVOLVER}^2 . These catalogs are equivalent to those in Douglass et al. (2023), but with the void and wall galaxies having K-corrections and E-corrections consistent with DESIVAST.

4.1. Comparison of Void Catalogs

To compare the sizes of voids across algorithms, we define an effective void radius as the radius corresponding to a sphere with the same volume as the overall void. The void volume is calculated with Monte-Carlo sampling of a bounding region around the void. The use of an effective void radius allows us to compare void sizes across algorithms that define voids differently.

The void counts and catalog properties for all three void catalogs are presented in Table 1 and Table 2. We compare the median effective radii, maximum effective radii, volume belonging to voids, and galaxies belonging to voids for each algorithm. We also include comparisons to the SDSS void catalogs from Douglass et al. (2023), with K-corrections and E-corrections described in Section 3.1.

We report uncertainties in void catalog properties due to cosmic variance and the magnitude systematic uncertainties of different surveys. We take the standard deviation of each catalog property across 25 AMTL mock

void catalogs σ_c to represent the combined effects of statistical uncertainty and cosmic variance for DESI. We do the same with 25 Horizon Run 4 mock void catalogs for SDSS.

To evaluate the systematic uncertainty due to magnitude, we take the width of the 68% confidence interval of the scatter at $M_r = -20$ in Figure 3 to represent the range over which the void-finding algorithm outputs vary due to the systematic uncertainties in the magnitudes of DESI and SDSS. We create versions of the DESIVAST and SDSS VAST catalogs with alternate magnitude cuts at the edges of the 68% interval range projected onto the axes of Figure 3: $M_r \leq -19.89$ and $M_r \leq -20.06$ for DESI, and $M_r \leq -19.94$ and $M_r \leq -20.11$ for SDSS. The differences in the void catalog properties between each alternate magnitude threshold and the main void catalogs produce asymmetric uncertainties σ_{\pm}^+ on the DESIVAST and SDSS VAST catalogs due to the scatter in the reported magnitudes.

For a given void catalog property, we report the uncertainty on a value x in as $x \pm \sigma_c(\text{stat.})_{-}^{+} \sigma_{\pm}^+(\text{sys.})$. In some instances, the values x_1 and x_2 for the alternate magnitude cut catalogs are both greater or lesser than the main catalog value x . In this case, we take the greater of the σ_{\pm}^+ uncertainties to represent one of the asymmetric uncertainties and report the other as 0.

When reporting median effective void radii, we account for the standard error of the median $\sigma_{\tilde{x}}$ as part of the statistical uncertainty. We report the uncertainty on a median value \tilde{x} as $\tilde{x} \pm (\sigma_s)(\text{stat.})_{-}^{+} \sigma_{\tilde{x}}^+(\text{sys.})$ where $\sigma_s^2 = \sigma_c^2 + \sigma_{\tilde{x}}^2$.

In Table 1, we present the void counts for DESIVAST DR1, the projected void counts for the complete DESI survey, and the median and maximum effective void radii. For DESIVAST DR1, we find 1,484 interior voids with VoidFinder, 386 with V_{REVOLVER}^2 , and 295 with V_{VIDE}^2 . Across all algorithms, over 60% of the detected voids are edge voids. This is due to the thin angular mask used to construct the DESIVAST DR1 catalog, which can be seen in Figure 2. We compare void counts with our SDSS void catalogs, where we find that despite the thin angular coverage of the DESIVAST DR1 mask, the DESIVAST void counts surpass or are comparable to the corresponding SDSS counts due to DESI’s improved redshift coverage, which allows for a distance limit in the volume-limited galaxy catalog of 677 Mpc h^{-1} , compared with the SDSS limit of 332 Mpc h^{-1} .

We use a BGS mock galaxy catalog to project the number of voids expected in the equivalent complete DESI survey version of our volume-limited catalog. We find around 15,000 interior voids in the VoidFinder catalog, and around 7,000 interior voids in each V^2 catalog.

In Figure 5, we show the physical distribution of voids in the complete DESI survey VoidFinder mock catalog. In contrast to the DESIVAST DR1 catalogs in Figure 4, we see that the complete DESI survey mock catalogs occupy a majority of the survey volume with a contiguous region of interior voids. This reflects the change in the relative number of edge and interior voids between DR1 and the complete DESI survey.

To reduce the effect of the survey boundaries on the statistical properties of voids, we report void properties within an interior fiducial volume V_{fid} . We exclude any region within 30 Mpc h^{-1} of the survey boundaries, removing regions near the DESIVAST DR1 mask edges and redshift limits. We likewise define a fiducial volume V_{fid} for SDSS by removing regions within 30 Mpc h^{-1} of the SDSS survey boundaries. Table 1 shows that the fiducial volume significantly reduces the number of edge voids that impact the reported void statistics, while allowing for the reported statistics to be calculated across a common volume for each algorithm.

The median and maximum effective radii for each algorithm of voids within our fiducial volume V_{fid} presented in Table 1. The median effective radii are 15.7 ± 0.1 (stat.) $_{-0.1}^{+0.0}$ (sys.) Mpc h^{-1} for VoidFinder, 19.9 ± 0.2 (stat.) $_{-0.8}^{+0.01}$ (sys.) Mpc h^{-1} for V_{REVOLVER}^2 , and 19.3 ± 0.3 (stat.) $_{-1.0}^{+0.0}$ (sys.) Mpc h^{-1} for V_{VIDE}^2 . The maximum effective radius is 31.3 (43.5, 55.9) Mpc h^{-1} for VoidFinder (V_{REVOLVER}^2 , V_{VIDE}^2). These trends reflect how the V^2 algorithm discovers larger voids than VoidFinder. For each algorithm, the median effective radii of the DESI and SDSS catalogs agree within their uncertainties.

In Table 2, we compare the void volume fraction, meaning the fraction of the survey volume in voids, and the fraction of galaxies in voids across catalogs. We again use our fiducial volume V_{fid} for this comparison. The void volume fractions are calculated by populating the fiducial volume with a grid of points spaced 1 Mpc h^{-1} apart and counting the relative number of grid points located within and exterior to voids. We find that DESIVAST voids fill a majority of the volume, with 63.0 ± 1.2 (stat.) $_{-2.2}^{+1.1}$ (sys.)% of the volume in VoidFinder Voids, 98.6 ± 0.2 (stat.) $_{-0.3}^{+0.0}$ (sys.)% of the volume in V_{REVOLVER}^2 voids, and 69.1 ± 3.0 (stat.) $_{-0.0}^{+1.2}$ (sys.)% of the volume in V_{VIDE}^2 voids. V^2 voids fill more of the universe than VoidFinder voids, and V_{REVOLVER}^2 identifies the near entirety of the volume as belonging to voids. These differences follow from the volume-filling

behavior of the V^2 algorithms and the post-processing cuts that we have applied to the catalogs. The SDSS void volume fractions agree with the DESI void volume fractions within uncertainties for all algorithms.

We select galaxies falling within our fiducial volume V_{fid} to compare the galaxy membership in voids across algorithms. We find that 22.8 ± 0.8 (stat.) $_{-2.1}^{+1.2}$ (sys.)% of galaxies are in VoidFinder voids, that 98.5 ± 0.3 (stat.) $_{-0.6}^{+0.0}$ (sys.)% of galaxies are V_{REVOLVER}^2 voids, and that 69.7 ± 2.6 (stat.) $_{-0.0}^{+0.7}$ (sys.)% of galaxies are V_{VIDE}^2 voids. The V^2 catalogs place a majority of the galaxies in voids, with V_{REVOLVER}^2 in particular identifying almost the entire galaxy population as belonging to voids. The high percentage of galaxies in V^2 voids are consequent to the volume-filling behavior of the V^2 algorithm and the post-processing cuts that we have applied to the catalogs. The fraction of galaxies within SDSS voids is consistent with the fraction of galaxies within DESI voids across all algorithms.

To further compare the different algorithms, we show in Table 2 the void volume common to VoidFinder and V_{VIDE}^2 , the void volume common to VoidFinder and V_{REVOLVER}^2 , and the void volume common to V_{REVOLVER}^2 and V_{VIDE}^2 . As before, we use the fiducial volume V_{fid} for this comparison. We find that compared to the 63.0 ± 1.2 (stat.) $_{-2.2}^{+1.1}$ (sys.)% of the fiducial volume within VoidFinder voids, a volume of 62.3 ± 1.2 (stat.) $_{-2.2}^{+1.1}$ (sys.)% is also within V_{REVOLVER}^2 voids, and a volume of 43.6 ± 2.0 (stat.) $_{-0.9}^{+1.5}$ (sys.)% is also within V_{VIDE}^2 voids. We find the entirety of the volume within V_{VIDE}^2 voids to be also within V_{REVOLVER}^2 voids. We also compare the agreement in galaxy membership within voids. We find that compared to the 22.8 ± 0.8 (stat.) $_{-2.1}^{+1.2}$ (sys.)% of galaxies within VoidFinder voids, a sample of 22.6 ± 0.8 (stat.) $_{-2.0}^{+1.2}$ (sys.)% is also within V_{REVOLVER}^2 voids, and a sample of 16.0 ± 0.8 (stat.) $_{-1.3}^{+1.2}$ (sys.)% is also within V_{VIDE}^2 voids. As with the volume comparison, we find the entirety of the galaxies within V_{VIDE}^2 voids to belong also to V_{REVOLVER}^2 voids. The results for SDSS are in agreement with those for DESI across all algorithms.

We observe overall consistency in the properties of DESIVAST and SDSS voids. We find that our SDSS void catalog properties at times differ from those reported in Douglass et al. (2023). This occurs for three reasons. First, our modified K-corrections and E-corrections for the NSA catalog change the void-finding output. Second, Douglass et al. (2023) places a 50% median void radius cut on their V_{REVOLVER}^2 catalog, whereas we use a 10 Mpc h^{-1} void radius cut. Third,

Table 1. DESI Void Catalog Comparisons

Catalog	VoidFinder	V ² /REVOLVER	V ² /VIDE
DESIVAST Void count (total/interior)	3,776 / 1,484	1,990 / 386	1,480 / 295
DESIVAST NGC Void Count (total/interior)	3,246 / 1,327	1,688 / 353	1,257 / 268
DESIVAST SGC Void Count (total/interior)	530 / 157	302 / 33	223 / 27
DESIVAST NGC Void Count in V_{fid} (total/interior)	930 / 860	547 / 298	397 / 222
DESIVAST SGC Void Count in V_{fid} (total/interior)	94 / 85	67 / 27	53 / 21
DESIVAST Complete Projected Void Count (total/interior)	18,181 / 15,385	8,635 / 6,789	9,648 / 7,290
SDSS DR7 Void Count (total/interior)	1,187 / 810	518 / 302	531 / 297
Median R_{eff} in V_{fid} [Mpc h ⁻¹] (DESI/SDSS)	$15.7 \pm 0.1^{+0.0}_{-0.1}$ / $15.9 \pm 0.1^{+0.1}_{-0.2}$	$19.9 \pm 0.2^{+0.01}_{-0.8}$ / $18.8 \pm 0.4^{+0.0}_{-0.4}$	$19.3 \pm 0.3^{+0.0}_{-1.0}$ / $18.0 \pm 0.5^{+0.2}_{-0.0}$
Maximum R_{eff} in V_{fid} [Mpc h ⁻¹] (DESI/SDSS)	31.3 / 30.2	43.5 / 42.1	55.9 / 56.5

NOTE—Properties of the DESIVAST DR1 void catalogs for VoidFinder, V_{REVOLVER}^2 , and V_{VIDE}^2 , with a fiducial volume V_{fid} used to account for survey edge effects. Projections for the completed DESI survey are given with AbacusSummit BGS mocks. Our SDSS catalogs serve as a modification to the work of [Douglass et al. \(2023\)](#). For the median radii \tilde{x} , we report statistical uncertainties σ_s , and asymmetric systematic uncertainties from galaxy magnitudes, σ_+ and σ_- , written as $\tilde{x} \pm \sigma_s^{+\sigma_+}$.

Table 2. Void-Finding Algorithm Comparisons

Algorithm	% V_{fid} in voids (DESI DR1)	% V_{fid} in voids (SDSS DR7)	% galaxies in voids (DESI DR1)	% galaxies in voids (SDSS DR7)
VoidFinder	$63.0 \pm 1.2^{+1.1}_{-2.2}$	$62.7 \pm 0.8^{+2.1}_{-1.0}$	$22.8 \pm 0.8^{+1.2}_{-2.1}$	$20.3 \pm 0.5^{+1.9}_{-0.9}$
V ² /REVOLVER	$98.6 \pm 0.2^{+0.0}_{-0.3}$	$99.0 \pm 0.4^{+0.3}_{-0.0}$	$98.5 \pm 0.3^{+0.0}_{-0.6}$	$98.3 \pm 0.6^{+0.5}_{-0.8}$
V ² /VIDE	$69.1 \pm 3.0^{+1.2}_{-0.0}$	$69.9 \pm 3.2^{+3.8}_{-0.0}$	$69.7 \pm 2.6^{+0.7}_{-0.0}$	$69.6 \pm 3.2^{+3.4}_{-0.0}$
VoidFinder \cap V ² /REVOLVER	$62.3 \pm 1.2^{+1.1}_{-2.2}$	$62.5 \pm 0.8^{+2.0}_{-1.0}$	$22.6 \pm 0.8^{+1.2}_{-2.0}$	$20.3 \pm 0.5^{+1.9}_{-1.0}$
VoidFinder \cap V ² /VIDE	$43.6 \pm 2.0^{+1.5}_{-0.9}$	$44.0 \pm 1.9^{+3.8}_{-0.7}$	$16.0 \pm 0.8^{+1.2}_{-1.3}$	$14.3 \pm 0.7^{+2.1}_{-0.6}$
V ² /VIDE \cap V ² /REVOLVER	$69.1 \pm 3.0^{+1.2}_{-0.0}$	$69.9 \pm 3.2^{+3.7}_{-0.0}$	$69.6 \pm 2.6^{+0.7}_{-0.0}$	$69.6 \pm 3.1^{+3.4}_{-0.0}$

NOTE—The void volume fractions and fraction of galaxies in voids for each void-finding algorithm, with a fiducial volume V_{fid} used to account for survey edge effects. We also show the agreement between each of the different algorithms. Our SDSS catalogs serve as a modification to the work of [Douglass et al. \(2023\)](#). For each value x , we report uncertainties due to cosmic variance, σ_c , and asymmetric uncertainties from galaxy magnitudes, σ_+ and σ_- , written as $x \pm \sigma_c^{+\sigma_+}$.

we use a 30 Mpc h⁻¹ border for defining a SDSS fiducial volume when calculating certain catalog properties. This border is used to prevent survey-edge effects from impacting the void catalog properties. Such a border was not used in [Douglass et al. \(2023\)](#).

4.2. The Volume Overlap of DESI and SDSS voids

We examine the consistency of our DESIVAST and SDSS void catalogs. We consider voids located within the 1308 deg² angular mask representing the DESIVAST-SDSS footprint overlap and within the

SDSS $z = 0.114$ redshift limit. To reduce survey edge effects, we apply a cut that removes regions within 10 Mpc h⁻¹ of the survey boundaries. We use a 10 Mpc h⁻¹ cut rather than the 30 Mpc h⁻¹ cut used for previous fiducial volumes, as the latter cut results in a vanishingly small number of voids. With our reduced edge cut, we expect DESI and SDSS survey edge effects to have a greater effect on the reported void statistics than with our previous comparisons.

We calculate the volume overlap of DESIVAST and SDSS voids that fall within the fiducial region. For

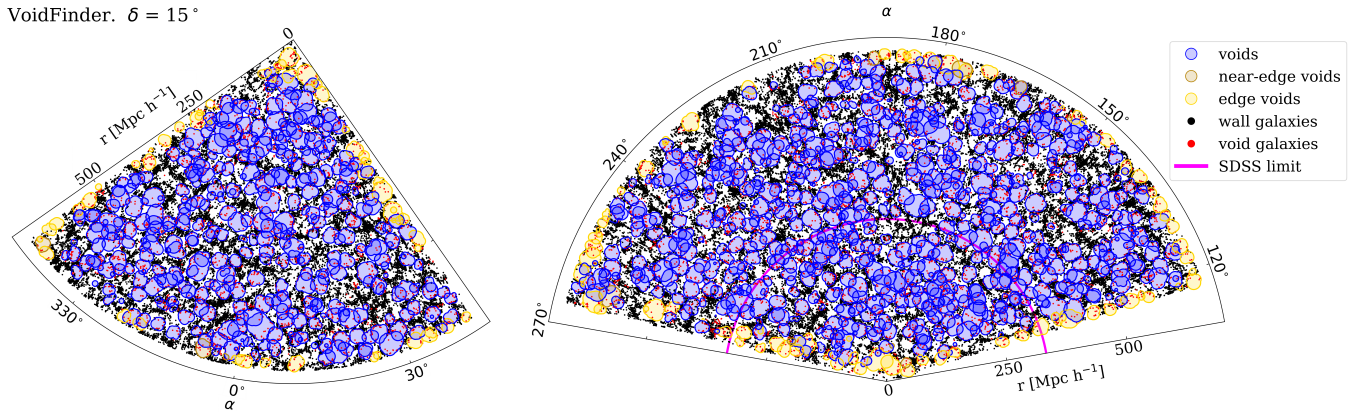


Figure 5. Slice plots of the projected VoidFinder volume-limited mock void catalog for the complete DESI survey. The catalog is built on an AbacusSummit BGS mock. A 10 Mpc h^{-1} thick slice of mock galaxies is plotted over the void distribution at a declination of $\delta = 15^\circ$. Void (wall) galaxies are shown in red (black). Edge (interior) voids are shown in yellow (blue). The SGC is shown on the left, and the NGC is shown on the right. For the NGC, we show a comparison with the Douglass et al. (2023) SDSS void catalog redshift limit (solid magenta line).

Table 3. Percentage of Fiducial Volume in Void Unions

Survey Region	VoidFinder (%)	V_{REVOLVER}^2 (%)	V_{VIDE}^2 (%)
DESI void \cap SDSS void	49.4	81.5	36.4
DESI void \cap SDSS non-void	10.4	4.7	24.6
DESI non-void \cap SDSS void	12.5	12.8	30.6
DESI non-void \cap SDSS non-void	27.7	1.1	8.6

NOTE—The percentage of the common DESI-SDSS fiducial volume found in the unions of void catalogs, for our three voidfinding algorithms. The first row gives the percentage of the fiducial volume within the union of DESI and SDSS voids. The second row gives the percentage of the fiducial volume found in DESI voids but not in SDSS voids. The third row gives the percentage of the fiducial volume found in SDSS voids but not in DESI voids. The fourth row gives the percentage of the fiducial volume exterior to both SDSS and DESI voids.

VoidFinder, we find that 49.4% of the targeted region is contained within both DESIVAST and SDSS voids, whereas 10.4% of the region is uniquely within DESI voids and 12.5% of the region is uniquely within SDSS voids. The remaining region is exterior to both void catalogs. We emphasize that this indicates an overall agreement in the performance of VoidFinder between DESI and SDSS, with 80-83% of the void volume in each catalog also belonging to voids in the other catalog. However, the remaining difference is significant, as we would expect a near 100% agreement in the ideal case.

Slice plots of the DESI and SDSS void catalogs in the targeted region are shown in Figure 6. We see that despite the 10% level difference in the volume overlap of

VoidFinder Combined Voids. $\delta = 1^\circ$

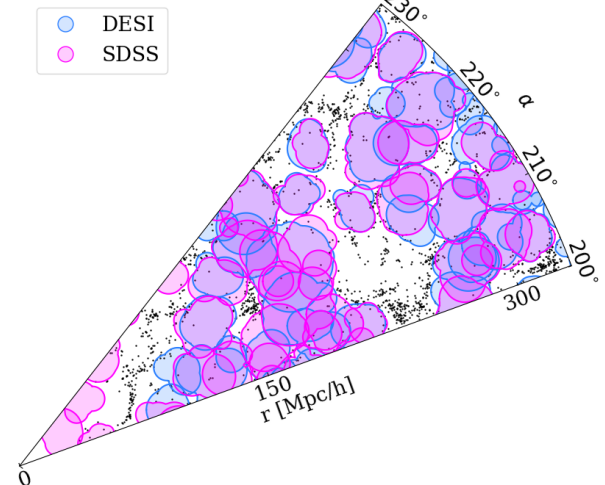


Figure 6. A slice plot of the VoidFinder void catalogs for DESI and SDSS. DESI voids are shown in cyan and SDSS voids are shown in magenta. A 10 Mpc h^{-1} thick slice of DESI galaxies is plotted over the void distribution in black at a declination of $\delta = 1^\circ$.

the catalogs, they identify the same general regions as voids.

For V_{VIDE}^2 , we find that 36.4% of the region is contained within both DESIVAST and SDSS voids. 24.6% of the region is uniquely in DESIVAST voids, and 30.6% of the region is uniquely within SDSS voids. 54-60% of the void volume in each catalog then also belongs to voids in the other catalog. For V_{REVOLVER}^2 , we find that 81.4% of the region is contained within both DESIVAST and SDSS voids. 4.7% of the region is uniquely in DESIVAST voids, and 12.8% of the region is uniquely within SDSS voids. 86-95% of the void volume in each

catalog then also belongs to voids in the other catalog. When using a 30 Mpc h^{-1} survey edge cut on the fiducial volume, the V_{REVOLVER}^2 void catalog is volume-filling, and we expect a near 100% agreement for V_{REVOLVER}^2 between DESI and SDSS. When using a 10 Mpc h^{-1} survey edge cut, the V_{REVOLVER}^2 pruning output contains more small voids that do not pass our 10 Mpc h^{-1} minimum void radius cut for the final catalog, resulting in greater disagreement for V_{REVOLVER}^2 between DESI and SDSS.

The differences in the volume overlap of the DESIVAST and SDSS void catalogs can be attributed in part to differing survey completeness. Our SDSS volume-limited catalog has more galaxies than our DESI volume-limited catalog, which changes the third nearest neighbor threshold used by VoidFinder and alters which galaxies are removed by the algorithm to grow holes in. Despite these changes, VoidFinder is able to identify the same general low-density regions as voids.

A higher survey completeness causes V^2 to better resolve watershed ridges, leading to a larger number of zones prior to pruning. For VIDE, better resolved watershed ridges also affect which adjacent zones meet the zone-linking criteria. This serves to change the quantity, size, and location of void candidates, which in turn affects which void candidates pass the central density cut that we apply to the VIDE catalog. We see a severe change in which regions of the survey volume VIDE identifies as voids for our different galaxy samples.

The differences in the volume overlap of the void catalogs may also be explained by DESIVAST and SDSS having different angular masks. Nearly all DESIVAST voids within $z \leq 0.114$ are edge voids. While most SDSS voids are not edge voids, the SDSS NGC mask defines a substantial part of the boundary of the DESIVAST-SDSS overlap footprint, thus introducing SDSS edge voids into the overlapping region. Both surveys then contribute edge voids into the shared fiducial volume. As the shapes of edge voids are uniquely impacted by their respective survey boundaries, a comparison of edge voids may contribute to the overall disagreement in the DESIVAST-SDSS void volume overlap.

We expect that the complete DESI survey, having an angular mask that encompasses the SDSS catalog, will provide a comparison of a larger number of interior voids between the two surveys. The survey angular masks will then no longer be as significant of a factor impacting the volume comparison.

We overall find that VoidFinder is more resilient than V_{VIDE}^2 to changes in survey design when it comes to consistently identifying the same regions as voids. We

find as expected that V_{REVOLVER}^2 consistently fills the majority of both survey volumes with voids.

5. CONCLUSION

We create three void catalogs over a volume-limited sample of DESI DR1 BGS Bright tracers within a redshift of $z \leq 0.24$. Our catalogs are built from two different algorithms: the sphere growing algorithm VoidFinder and the watershed algorithm V^2 with VIDE and REVOLVER pruning methods. As result of the thin survey mask of DESI DR1, our catalogs consist mainly of edge voids which occur along the survey boundaries. We find 1,484 non-edge voids in the VoidFinder catalog, 386 in the V_{REVOLVER}^2 catalog, and 295 in the V_{VIDE}^2 catalog. Our VoidFinder voids are smaller, more numerous, and occupy less of the survey volume than our V^2 voids, consistent with the well-understood behavior of each algorithm. We find that void catalog properties such as void volume fractions and the fraction of galaxies within voids are consistent between DESI and SDSS voids.

We find that the volume overlap agreement between DESI and SDSS has significant differences for all algorithms, particularly for V_{VIDE}^2 . We propose differences in the DESI and SDSS survey design as the reason for this disagreement. We note that despite the disagreement in the volume overlap, VoidFinder is able to identify the same general low density regions as voids.

We present our DESI-SDSS void comparison as a precursor to the complete DESI survey, where we will be able to compare a larger, contiguous region of both surveys. Our future catalogs will also extend beyond a volume-limited BGS Bright sample to include the full set of DESI tracers, taking advantage of the wide range of cosmic history that DESI probes.

DESIVAST DR1 is the first publicly released DESI void catalog. With DESIVAST, we will enable new void-based studies of cosmology and astrophysics.

6. ACKNOWLEDGEMENTS

We would like to thank Michael Vogeley for his expertise and for useful discussions regarding void-finding and

Table 4. VoidFinder Maximal Spheres HDU Columns

X	Y	Z	RADIUS	VOID	EDGE	R	RA	DEC	R_EFF	R_EFF_UNCERT
Mpc h ⁻¹	Mpc h ⁻¹	Mpc h ⁻¹	Mpc h ⁻¹			Mpc h ⁻¹	deg	deg	Mpc h ⁻¹	Mpc h ⁻¹
(1)	(2)	(3)	(4)	(5)	(6)	(7)	(8)	(9)	(10)	(11)
-624.51	-133.79	-85.41	24.04	0	1	644.37	192.09	-7.62	30.52	0.108
-224.19	-355.12	59.92	23.98	1	1	424.22	237.74	8.12	31.32	0.116
-140.92	-585.75	152.59	23.51	2	1	621.49	256.47	14.21	30.35	0.112

NOTE—The column organization of the VoidFinder maximal spheres HDU, with each row corresponding to an example maximal sphere. Columns include (1–3) the Cartesian coordinates of the sphere’s center, (4) the sphere’s radius, (5) a flag identifying each sphere’s void, (6) a boolean edge-flag indicating if a void is an edge voids, (7–9) the spherical coordinates of the sphere’s center, and (10–11) the void’s effective radius and its uncertainty. We show the first three voids in our VoidFinder catalog. The full catalog is published online.

Table 5. V² Voids HDU Columns

VOID	X	Y	Z	REDSHIFT	RA	DEC	RADIUS	X1...	TOT_AREA	EDGE_AREA
	Mpc h ⁻¹	Mpc h ⁻¹	Mpc h ⁻¹		deg	deg	Mpc h ⁻¹	Mpc h ⁻¹	(Mpc h ⁻¹) ²	(Mpc h ⁻¹) ²
(1)	(2)	(3)	(4)	(5)	(6)	(7)	(8)	(9-17)	(18)	(19)
0	-217.74	442.78	238.31	0.192	116.19	25.78	29.32	-4.13...	41538.4	14623.07
1	-36.36	-269.64	85.79	0.0974	262.32	17.5	25.1	-5.35...	27470.71	8740.29
2	-203.17	-562.61	72.87	0.212	250.14	6.95	43.57	-8.36...	76674.29	4926.75

NOTE—The column organization of the V² voids HDU, with each row corresponding to an example void. Columns include (1) a flag identifying each void, (2–4) the Cartesian coordinates of the void’s center, (5–7) the spherical coordinates of the void’s center, (8) the void’s effective radius, (9–17) the three components [X–Z] of the three ellipsoid axes [1–3] of the best fit ellipsoid, (18) the void’s surface area, and (19) the void’s surface area touching the survey boundary. We show the first three voids in our V_{VIDE}² catalog. The full catalog is published online.

Table 6. VoidFinder Holes HDU Columns

X	Y	Z	RADIUS	VOID
Mpc h ⁻¹	Mpc h ⁻¹	Mpc h ⁻¹	Mpc h ⁻¹	
(1)	(2)	(3)	(4)	(5)
-624.51	-133.79	-85.41	24.04	0
-224.19	-355.12	59.92	23.98	1
-224.23	-355.06	59.8	23.97	1

NOTE—The column organization of the VoidFinder hole spheres HDU, with each row corresponding to an example hole. Columns include (1–3) the Cartesian coordinates of the sphere’s center, (4) the sphere’s radius, (5) a flag identifying each sphere’s void. We show the first three holes in our VoidFinder catalog. The full catalog is published online.

void analysis. We would also like to thank Steve O’Neill for writing a significant portion of the VAST VoidFinder codebase. We acknowledge support from the United States Department of Energy grant DE-SC0008475, Experimental Studies of Elementary Particles and Fields for H. Rincon, S. BenZvi and D. Veyrat. We acknowledge support from grant 62177 from the John Templeton Foundation for H. Rincon, K. Douglass, and D. Veyrat.

This material is based upon work supported by the U.S. Department of Energy (DOE), Office of Science, Office of High-Energy Physics, under Contract No. DE-AC02-05CH11231, and by the National Energy Research Scientific Computing Center, a DOE Office of Science User Facility under the same contract. Additional support for DESI was provided by the U.S. National Science Foundation (NSF), Division of Astronomical Sciences under Contract No. AST-0950945 to the NSF’s National Optical-Infrared Astronomy Re-

Table 7. V^2 Zones HDU Columns

ZONE	VOID0	VOID1
(1)	(2)	(3)
0	1256	1256
1	-1	-1
2	-1	-1

NOTE—The column organization of the V^2 zones HDU, with each row corresponding to an example zone. Columns include (1) the zone ID, (2) the ID of the zone’s smallest containing void, and (3), the ID of the zone’s largest containing void. Values of -1 indicate that a zone does not belong to any void. We show the first three zones in our V_{VIDE}^2 catalog. The full catalog is published online.

search Laboratory; the Science and Technology Facilities Council of the United Kingdom; the Gordon and Betty Moore Foundation; the Heising-Simons Foundation; the French Alternative Energies and Atomic Energy Commission (CEA); the National Council of Humanities, Science and Technology of Mexico (CONACYT); the Ministry of Science, Innovation and Universities of Spain (MICIU/AEI/10.13039/501100011033), and by the DESI Member Institutions: <https://www.desi.lbl.gov/collaborating-institutions>. Any opinions, findings, and conclusions or recommendations expressed in this material are those of the author(s) and do not necessarily reflect the views of the U. S. National Science Foundation, the U. S. Department of Energy, or any of the listed funding agencies.

The authors are honored to be permitted to conduct scientific research on Iolkam Du’ag (Kitt Peak), a mountain with particular significance to the Tohono O’odham Nation.

Funding for the SDSS and SDSS-II has been provided by the Alfred P. Sloan Foundation, the Participating Institutions, the National Science Foundation, the U.S. Department of Energy, the National Aeronautics and Space Administration, the Japanese Monbukagakusho, the Max Planck Society, and the Higher Education Funding Council for England. The SDSS website is <http://www.sdss.org/>.

The SDSS is managed by the Astrophysical Research Consortium for the Participating Institutions. The Participating Institutions are the American Museum of Natural History, Astrophysical Institute Potsdam, University of Basel, University of Cambridge, Case Western

Reserve University, University of Chicago, Drexel University, Fermilab, the Institute for Advanced Study, the Japan Participation Group, Johns Hopkins University, the Joint Institute for Nuclear Astrophysics, the Kavli Institute for Particle Astrophysics and Cosmology, the Korean Scientist Group, the Chinese Academy of Sciences (LAMOST), Los Alamos National Laboratory, the Max Planck Institute for Astronomy (MPIA), the Max Planck Institute for Astrophysics (MPA), New Mexico State University, Ohio State University, University of Pittsburgh, University of Portsmouth, Princeton University, the United States Naval Observatory, and the University of Washington.

7. APPENDIX

7.1. Void Catalog File Descriptions for DESIVAST

Our three void catalogs will be included in DESIVAST, a value added catalog to be released with DESI DR1. In DESIVAST, the void catalogs are stored as FITS files and are separated into NGC and SGC catalogs. The principal file organization identifying unique voids for each algorithm is presented in Table 4 for VoidFinder and Table 5 for V^2 .

For VoidFinder, the void information is separated into two FITS Header Data Units (HDU): a maximal spheres HDU and a holes HDU. The maximal spheres HDU is exemplified in Table 4. The HDU contains the location of the maximal spheres in Cartesian and spherical coordinates, the radius of the maximal spheres, a flag identifying the void each maximal sphere belongs to, an edge flag determining if each maximal sphere belongs to an edge or interior void, the effective radius of the void that each maximal sphere belongs to, and the uncertainty in the effective radius calculation. The holes HDU is exemplified in Table 6. The HDU contains the Cartesian coordinates of the holes, the hole radii, and a flag identifying with void each hole belongs to.

The V^2 catalog information is divided among five HDUs. Among these, the voids HDU, exemplified in Table 5, includes the center of voids as the volume-weighted sum of their Voronoi cells.

$$\vec{x}_{\text{center}} = V_{\text{void}}^{-1} \sum_i \vec{x}_i V_i \quad (1)$$

Here V_{void} is the total void volume and i sums over the cells to access their positions and volumes. The voids HDU contains a flag identifying each void, the weighted centers of each void in spherical and Cartesian coordinates, the effective radii of the voids, the axes of ellipsoids fitted to each void, the surface area of each void, and the partial surface area of each void that is adjacent to the survey boundaries. The zones HDU, exemplified

Table 8. V^2 Galaxies HDU Columns

GAL	TARGET	X	Y	Z	ZONE	DEPTH	EDGE	OUT
		Mpc h ⁻¹	Mpc h ⁻¹	Mpc h ⁻¹				
(1)	(2)	(3)	(4)	(5)	(6)	(7)	(8)	(9)
0	39627540897202342	-549.38	210.35	-105.09	2961	0	1	0
1	39627540897202561	-313.07	119.55	-60.12	2961	0	1	0
2	39627540897202679	-521.83	198.87	-99.74	2961	0	1	0

NOTE—The column organization of the V^2 galaxies HDU, with each row corresponding to an example galaxy. Columns include (1) the V^2 -specified galaxy ID, (2) the original survey-specified galaxy ID, (3–5) the Cartesian coordinates of the galaxy, (6) the ID of the zone containing the galaxy, (7) the minimum number of adjacent cells between the galaxy and the edge of its zone, (8) a boolean flag indicating if the galaxy’s cell is fully contained by the survey mask, and (9) a boolean flag indicating if the galaxy is within the survey mask. We show the first three galaxies in our V^2_{VIDE} catalog. The full catalog is published online.

Table 9. V^2 Galaxy Visualization HDU Columns

GID	G2V	G2V2
1	2	3
0	-1	-1
1	-1	-1
2	-1	-1

NOTE—The column organization of the V^2 galaxy visualization HDU, with each row corresponding to an example galaxy. Columns include (1) the galaxy ID, (2) the ID of the galaxy’s containing void, and (3), the ID of the void containing the galaxy’s nearest neighbor galaxy. Values of -1 indicate that a galaxy does not belong to a void. We show the first three galaxies in our V^2_{VIDE} catalog. The full catalog is published online.

in Table 7, contains a flag uniquely identifying each zone as well as the smallest and largest voids in the void hierarchy that each zone belongs to. The galaxies HDU, exemplified in Table 8, contains a flag uniquely identifying each galaxy, the galaxy ID assigned by the original survey, the Cartesian coordinates of the galaxy, a flag for which zone each galaxy belongs to, the number of cells between a galaxy’s cell and the edge of its zone, a flag for whether the galaxy’s cell extends past the survey boundaries, and a flag for whether the galaxy itself is outside the survey boundaries. The galaxy visualization HDU,

Table 10. V^2 Triangles HDU Columns

VOID_ID	N_X...	P1_X...
	Mpc h ⁻¹	Mpc h ⁻¹
	(2–4)	(5–13)
1	0.838...	-29.11...
1	-0.497...	-33.54...
1	-0.497...	-33.54...

NOTE—The column organization of the V^2 triangles HDU, with each row corresponding to a triangle. Columns include (1) the ID of the void containing the triangle, (2–4) the three components [X–Z] of the triangle’s normal vector, (5–13) the three components [X–Z] of the triangle’s three vertices [1–3]. We show the first three triangles in our V^2_{VIDE} catalog. The full catalog is published online.

exemplified in Table 9, contains a flag uniquely identifying each galaxy, a flag for which void each galaxy belongs to, and a flag for which void each galaxy’s nearest neighbor galaxy belongs to. The triangles HDU, exemplified in Table 10, describes the triangles that may be used to visualize the voids in representative figures. The HDU columns include a flag for which void each triangle belongs to, three columns for the components of each triangle’s normal vector, and nine columns for the components of each triangle’s vertices.

7.2. Data Access

The DESIVAST value added catalogs will be published online with the release of DESI DR1. The data

points used for all figures in this paper will be published online with the release of DESI DR1.

REFERENCES

- Abazajian, K. N., Adelman-McCarthy, J. K., Agüeros, M. A., et al. 2009, *ApJS*, 182, 543, doi: [10.1088/0067-0049/182/2/543](https://doi.org/10.1088/0067-0049/182/2/543)
- Abdurro'uf, Accetta, K., Aerts, C., et al. 2022, *ApJS*, 259, 35, doi: [10.3847/1538-4365/ac4414](https://doi.org/10.3847/1538-4365/ac4414)
- Achitouv, I. 2019, *PhRvD*, 100, 123513, doi: [10.1103/PhysRevD.100.123513](https://doi.org/10.1103/PhysRevD.100.123513)
- Alcock, C., & Paczynski, B. 1979, *Nature*, 281, 358, doi: [10.1038/281358a0](https://doi.org/10.1038/281358a0)
- Bailey et al. 2024
- Bernardeau, F., Colombi, S., Gaztañaga, E., & Scoccimarro, R. 2002, *PhR*, 367, 1, doi: [10.1016/S0370-1573\(02\)00135-7](https://doi.org/10.1016/S0370-1573(02)00135-7)
- Blanton, M. R., Kazin, E., Muna, D., Weaver, B. A., & Price-Whelan, A. 2011, *AJ*, 142, 31, doi: [10.1088/0004-6256/142/1/31](https://doi.org/10.1088/0004-6256/142/1/31)
- Cautun, M., van de Weygaert, R., Jones, B. J. T., & Frenk, C. S. 2014, *MNRAS*, 441, 2923, doi: [10.1093/mnras/stu768](https://doi.org/10.1093/mnras/stu768)
- Chaussidon, E., Yèche, C., Palanque-Delabrouille, N., et al. 2023, *ApJ*, 944, 107, doi: [10.3847/1538-4357/acb3c2](https://doi.org/10.3847/1538-4357/acb3c2)
- Collaboration, D., Adame, A. G., Aguilar, J., et al. 2024, *The Astronomical Journal*, 168, 58, doi: [10.3847/1538-3881/ad3217](https://doi.org/10.3847/1538-3881/ad3217)
- Contarini, S., Pisani, A., Hamaus, N., et al. 2023, *ApJ*, 953, 46, doi: [10.3847/1538-4357/acde54](https://doi.org/10.3847/1538-4357/acde54)
- Contarini, S., Verza, G., Pisani, A., et al. 2022, *A&A*, 667, A162, doi: [10.1051/0004-6361/202244095](https://doi.org/10.1051/0004-6361/202244095)
- Demchenko, V., Cai, Y.-C., Heymans, C., & Peacock, J. A. 2016, *MNRAS*, 463, 512, doi: [10.1093/mnras/stw2030](https://doi.org/10.1093/mnras/stw2030)
- DESI Collaboration, Aghamousa, A., Aguilar, J., et al. 2016a, arXiv e-prints, arXiv:1611.00036, doi: [10.48550/arXiv.1611.00036](https://doi.org/10.48550/arXiv.1611.00036)
- . 2016b, arXiv e-prints, arXiv:1611.00037, doi: [10.48550/arXiv.1611.00037](https://doi.org/10.48550/arXiv.1611.00037)
- DESI Collaboration, Abareshi, B., Aguilar, J., et al. 2022, *AJ*, 164, 207, doi: [10.3847/1538-3881/ac882b](https://doi.org/10.3847/1538-3881/ac882b)
- DESI Collaboration, Adame, A. G., Aguilar, J., et al. 2024a, *AJ*, 167, 62, doi: [10.3847/1538-3881/ad0b08](https://doi.org/10.3847/1538-3881/ad0b08)
- DESI Collaboration, et al. 2024b, DESI 2024 I: Data Release 1 of the Dark Energy Spectroscopic Instrument, preparation
- . 2024c, DESI 2024 II: Two Point Clustering Measurements and Validation, preparation
- DESI Collaboration, Adame, A. G., Aguilar, J., et al. 2024d, arXiv e-prints, arXiv:2404.03000, doi: [10.48550/arXiv.2404.03000](https://doi.org/10.48550/arXiv.2404.03000)
- . 2024e, arXiv e-prints, arXiv:2404.03001, doi: [10.48550/arXiv.2404.03001](https://doi.org/10.48550/arXiv.2404.03001)
- DESI Collaboration, et al. 2024f, DESI 2024 V: Fullshape from Galaxies and Quasars, preparation
- . 2024g, DESI 2024 VII: Cosmological Constraints from the Fullshape Measurements, preparation
- Dey, A., Schlegel, D. J., Lang, D., et al. 2019, *AJ*, 157, 168, doi: [10.3847/1538-3881/ab089d](https://doi.org/10.3847/1538-3881/ab089d)
- Douglass, K. A., Veyrat, D., & BenZvi, S. 2023, *ApJS*, 265, 7, doi: [10.3847/1538-4365/acabcf](https://doi.org/10.3847/1538-4365/acabcf)
- Dunkley, J., Komatsu, E., Nolta, M. R., et al. 2009, *ApJS*, 180, 306, doi: [10.1088/0067-0049/180/2/306](https://doi.org/10.1088/0067-0049/180/2/306)
- Eisenstein, D. J., Annis, J., Gunn, J. E., et al. 2001, *AJ*, 122, 2267, doi: [10.1086/323717](https://doi.org/10.1086/323717)
- El-Ad, H., & Piran, T. 1997, *ApJ*, 491, 421, doi: [10.1086/304973](https://doi.org/10.1086/304973)
- Fukugita, M., Ichikawa, T., Gunn, J. E., et al. 1996, *AJ*, 111, 1748, doi: [10.1086/117915](https://doi.org/10.1086/117915)
- Garrison, L. H., Eisenstein, D. J., Ferrer, D., Maksimova, N. A., & Pinto, P. A. 2021, *MNRAS*, 508, 575, doi: [10.1093/mnras/stab2482](https://doi.org/10.1093/mnras/stab2482)
- Gregory, S. A., & Thompson, L. A. 1978, *ApJ*, 222, 784, doi: [10.1086/156198](https://doi.org/10.1086/156198)
- Gunn, J. E., Siegmund, W. A., Mannery, E. J., et al. 2006, *AJ*, 131, 2332, doi: [10.1086/500975](https://doi.org/10.1086/500975)
- Guy, J., Bailey, S., Kremin, A., et al. 2023a, *AJ*, 165, 144, doi: [10.3847/1538-3881/acb212](https://doi.org/10.3847/1538-3881/acb212)
- . 2023b, *AJ*, 165, 144, doi: [10.3847/1538-3881/acb212](https://doi.org/10.3847/1538-3881/acb212)
- Hadzhiyska, B., Eisenstein, D., Bose, S., Garrison, L. H., & Maksimova, N. 2022, *MNRAS*, 509, 501, doi: [10.1093/mnras/stab2980](https://doi.org/10.1093/mnras/stab2980)
- Hahn, C., Wilson, M. J., Ruiz-Macias, O., et al. 2023, *AJ*, 165, 253, doi: [10.3847/1538-3881/acff8](https://doi.org/10.3847/1538-3881/acff8)
- Hamaus, N., Pisani, A., Choi, J.-A., et al. 2020, *JCAP*, 2020, 023, doi: [10.1088/1475-7516/2020/12/023](https://doi.org/10.1088/1475-7516/2020/12/023)
- Hong, S. E., Park, C., & Kim, J. 2016, *ApJ*, 823, 103, doi: [10.3847/0004-637X/823/2/103](https://doi.org/10.3847/0004-637X/823/2/103)
- Hoyle, F., & Vogeley, M. S. 2002, *The Astrophysical Journal*, 566, 641–651, doi: [10.1086/338340](https://doi.org/10.1086/338340)
- Jõeveer, M., Einasto, J., & Tago, E. 1978, *MNRAS*, 185, 357, doi: [10.1093/mnras/185.2.357](https://doi.org/10.1093/mnras/185.2.357)

- Jennings, E., Li, Y., & Hu, W. 2013, *MNRAS*, 434, 2167, doi: [10.1093/mnras/stt1169](https://doi.org/10.1093/mnras/stt1169)
- Kim, J., Park, C., L’Huillier, B., & Hong, S. E. 2015, *Journal of Korean Astronomical Society*, 48, 213, doi: [10.5303/JKAS.2015.48.4.213](https://doi.org/10.5303/JKAS.2015.48.4.213)
- Lasker, J., Carnero Rosell, A., Myers, A. D., et al. 2024, arXiv e-prints, arXiv:2404.03006, doi: [10.48550/arXiv.2404.03006](https://doi.org/10.48550/arXiv.2404.03006)
- Levi, M., Bebek, C., Beers, T., et al. 2013, arXiv e-prints, arXiv:1308.0847, doi: [10.48550/arXiv.1308.0847](https://doi.org/10.48550/arXiv.1308.0847)
- Libeskind, N. I., van de Weygaert, R., Cautun, M., et al. 2018, *MNRAS*, 473, 1195, doi: [10.1093/mnras/stx1976](https://doi.org/10.1093/mnras/stx1976)
- Maksimova, N. A., Garrison, L. H., Eisenstein, D. J., et al. 2021, *MNRAS*, 508, 4017, doi: [10.1093/mnras/stab2484](https://doi.org/10.1093/mnras/stab2484)
- Mao, Q., Berlind, A. A., Scherrer, R. J., et al. 2017, *ApJ*, 835, 161, doi: [10.3847/1538-4357/835/2/161](https://doi.org/10.3847/1538-4357/835/2/161)
- McNaught-Roberts, T., Norberg, P., Baugh, C., et al. 2014, *MNRAS*, 445, 2125, doi: [10.1093/mnras/stu1886](https://doi.org/10.1093/mnras/stu1886)
- Miller, T. N., Doel, P., Gutierrez, G., et al. 2023, arXiv e-prints, arXiv:2306.06310, doi: [10.48550/arXiv.2306.06310](https://doi.org/10.48550/arXiv.2306.06310)
- Moustakas, J. 2024, in preparation
- Moustakas, J., Scholte, D., Dey, B., & Khederlarian, A. 2023, *FastSpecFit: Fast spectral synthesis and emission-line fitting of DESI spectra*, Astrophysics Source Code Library, record ascl:2308.005
- Nadathur, S. 2016, *MNRAS*, 461, 358, doi: [10.1093/mnras/stw1340](https://doi.org/10.1093/mnras/stw1340)
- Nadathur, S., Carter, P. M., Percival, W. J., Winther, H. A., & Bautista, J. E. 2019, *PhRvD*, 100, 023504, doi: [10.1103/PhysRevD.100.023504](https://doi.org/10.1103/PhysRevD.100.023504)
- Neyrinck, M. C. 2008, *MNRAS*, 386, 2101, doi: [10.1111/j.1365-2966.2008.13180.x](https://doi.org/10.1111/j.1365-2966.2008.13180.x)
- Pan, D. C., Vogeley, M. S., Hoyle, F., Choi, Y.-Y., & Park, C. 2012, *MNRAS*, 421, 926, doi: [10.1111/j.1365-2966.2011.20197.x](https://doi.org/10.1111/j.1365-2966.2011.20197.x)
- Patiri, S. G., Prada, F., Holtzman, J., Klypin, A., & Betancort-Rijo, J. 2006, *MNRAS*, 372, 1710, doi: [10.1111/j.1365-2966.2006.10975.x](https://doi.org/10.1111/j.1365-2966.2006.10975.x)
- Perico, E. L. D., Voivodic, R., Lima, M., & Mota, D. F. 2019, *A&A*, 632, A52, doi: [10.1051/0004-6361/201935949](https://doi.org/10.1051/0004-6361/201935949)
- Pisani, A., Sutter, P. M., Hamaus, N., et al. 2015, *PhRvD*, 92, 083531, doi: [10.1103/PhysRevD.92.083531](https://doi.org/10.1103/PhysRevD.92.083531)
- Pisani, A., Massara, E., Spergel, D. N., et al. 2019, *BAAS*, 51, 40, doi: [10.48550/arXiv.1903.05161](https://doi.org/10.48550/arXiv.1903.05161)
- Planck Collaboration, Aghanim, N., Akrami, Y., et al. 2020, *A&A*, 641, A6, doi: [10.1051/0004-6361/201833910](https://doi.org/10.1051/0004-6361/201833910)
- Raichoor, A., Moustakas, J., Newman, J. A., et al. 2023, *AJ*, 165, 126, doi: [10.3847/1538-3881/acb213](https://doi.org/10.3847/1538-3881/acb213)
- Richards, G. T., Fan, X., Newberg, H. J., et al. 2002, *AJ*, 123, 2945, doi: [10.1086/340187](https://doi.org/10.1086/340187)
- Schlafly, E. F., Kirkby, D., Schlegel, D. J., et al. 2023, *AJ*, 166, 259, doi: [10.3847/1538-3881/ad0832](https://doi.org/10.3847/1538-3881/ad0832)
- Sheth, R. K., & van de Weygaert, R. 2004, *MNRAS*, 350, 517, doi: [10.1111/j.1365-2966.2004.07661.x](https://doi.org/10.1111/j.1365-2966.2004.07661.x)
- Silber, J. H., Fagrelus, P., Fanning, K., et al. 2023, *AJ*, 165, 9, doi: [10.3847/1538-3881/ac9ab1](https://doi.org/10.3847/1538-3881/ac9ab1)
- Song, Y., Xiong, Q., Gong, Y., et al. 2024, arXiv e-prints, arXiv:2402.05492, doi: [10.48550/arXiv.2402.05492](https://doi.org/10.48550/arXiv.2402.05492)
- Springel, V., Frenk, C. S., & White, S. D. M. 2006, *Nature*, 440, 1137, doi: [10.1038/nature04805](https://doi.org/10.1038/nature04805)
- Strauss, M. A., Weinberg, D. H., Lupton, R. H., et al. 2002, *AJ*, 124, 1810, doi: [10.1086/342343](https://doi.org/10.1086/342343)
- Sutter, P. M., Lavaux, G., Hamaus, N., et al. 2014a, *MNRAS*, 442, 462, doi: [10.1093/mnras/stu893](https://doi.org/10.1093/mnras/stu893)
- Sutter, P. M., Lavaux, G., Wandelt, B. D., & Weinberg, D. H. 2012a, *ApJ*, 761, 187, doi: [10.1088/0004-637X/761/2/187](https://doi.org/10.1088/0004-637X/761/2/187)
- . 2012b, *ApJ*, 761, 44, doi: [10.1088/0004-637X/761/1/44](https://doi.org/10.1088/0004-637X/761/1/44)
- Sutter, P. M., Pisani, A., Wandelt, B. D., & Weinberg, D. H. 2014b, *MNRAS*, 443, 2983, doi: [10.1093/mnras/stu1392](https://doi.org/10.1093/mnras/stu1392)
- Sutter, P. M., Lavaux, G., Hamaus, N., et al. 2015, *Astronomy and Computing*, 9, 1, doi: [10.1016/j.ascom.2014.10.002](https://doi.org/10.1016/j.ascom.2014.10.002)
- van de Weygaert, R. 2014, *Proceedings of the International Astronomical Union*, 11, 493–523, doi: [10.1017/S1743921316010504](https://doi.org/10.1017/S1743921316010504)
- van de Weygaert, R., & Platen, E. 2011, *International Journal of Modern Physics: Conference Series*, 01, 41, doi: [10.1142/S2010194511000092](https://doi.org/10.1142/S2010194511000092)
- Veyrat, D., Douglass, K. A., & BenZvi, S. 2023, *ApJ*, 958, 59, doi: [10.3847/1538-4357/acf4f5](https://doi.org/10.3847/1538-4357/acf4f5)
- Voivodic, R., Lima, M., Llinares, C., & Mota, D. F. 2017, *PhRvD*, 95, 024018, doi: [10.1103/PhysRevD.95.024018](https://doi.org/10.1103/PhysRevD.95.024018)
- York, D. G., Adelman, J., Anderson, John E., J., et al. 2000, *AJ*, 120, 1579, doi: [10.1086/301513](https://doi.org/10.1086/301513)
- Zaidouni, F., Veyrat, D., Douglass, K. A., & BenZvi, S. 2024, arXiv e-prints, arXiv:2403.20008, doi: [10.48550/arXiv.2403.20008](https://doi.org/10.48550/arXiv.2403.20008)
- Zhou, R., Dey, B., Newman, J. A., et al. 2023, *AJ*, 165, 58, doi: [10.3847/1538-3881/aca5fb](https://doi.org/10.3847/1538-3881/aca5fb)